Figure S1, related to Figure 1: Cryo-EM image processing flow chart.

Rio2-TAP Pre40S

Relion Refine: K=1

144,902 particles, 15.6 Å

Euler Angle Normalization: ~33% culled

Kept: 97,265 part, 16.3 Å

Relion Masked Classify Mask = All AF sites

- Co-purified Mature 40S-Rio2
- Degraded Pre40S
- Poorly Classifying

Relion Unmasked Refine

Relion Masked Classify Mask = core only

- Incomplete 18S rRNA

Unmasked Frealign Refine

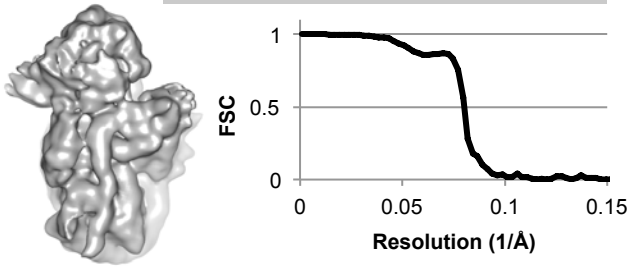

Rio2-TAP Final, 51,496 particles, 11.5 Å

Ltv1-TAP Pre40S

Relion Refine: K=1

177,379 particles, 13.5 Å

Euler Angle Normalization: ~51% culled

Kept: 80,346 part, 15.2 Å

Unmasked Frealign Refine

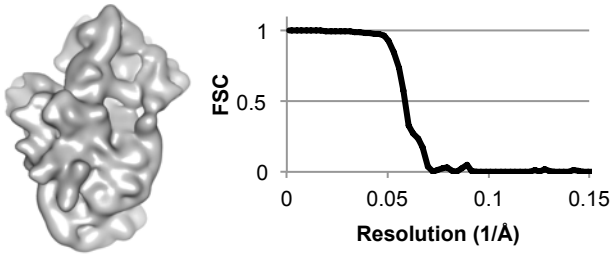

Ltv1-TAP Final: 80,346 particles, 14.8 Å

Unmasked Frealign Refine

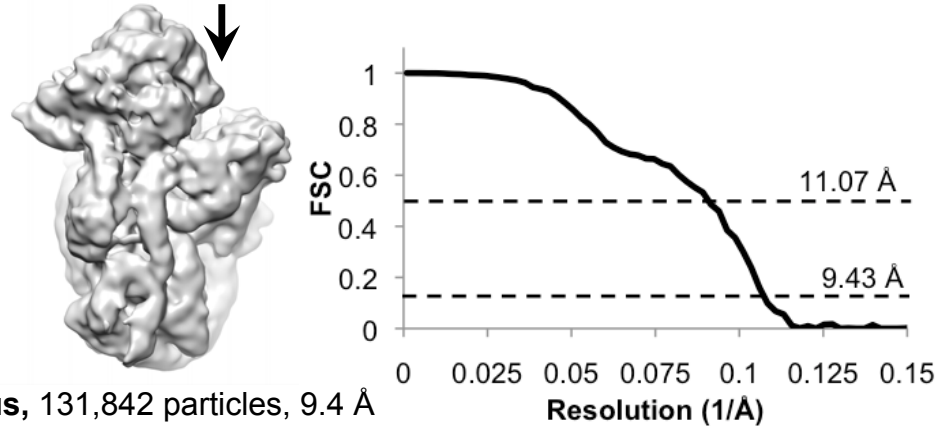

Rio2-TAP / Ltv1-TAP Consensus, 131,842 particles, 9.4 Å

Legend: Serial 3D classification normalized angular orientations and identified a stable core.

Figure S2, related to Figures 2-4: Focused classification of Rio2-TAP interface AFs

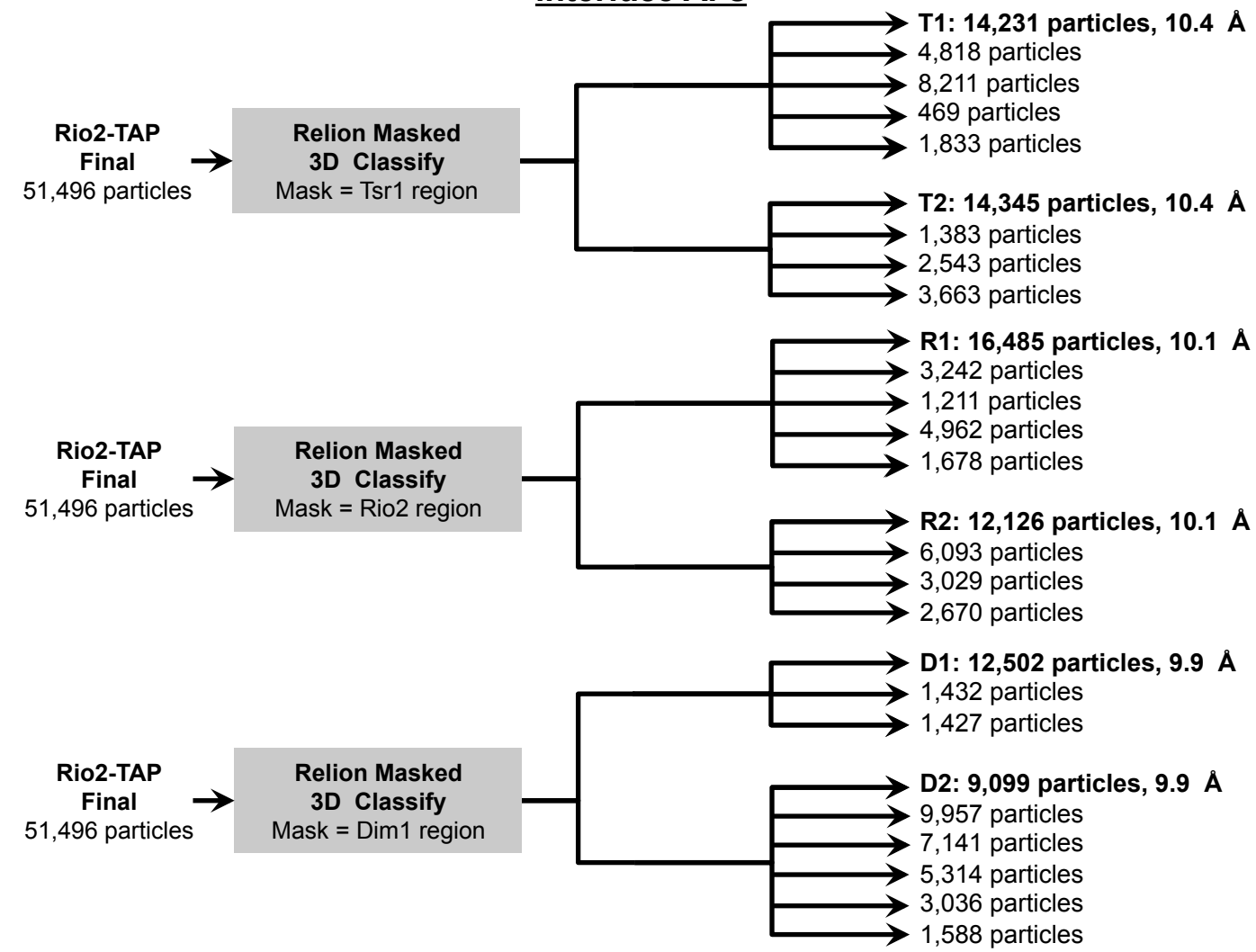

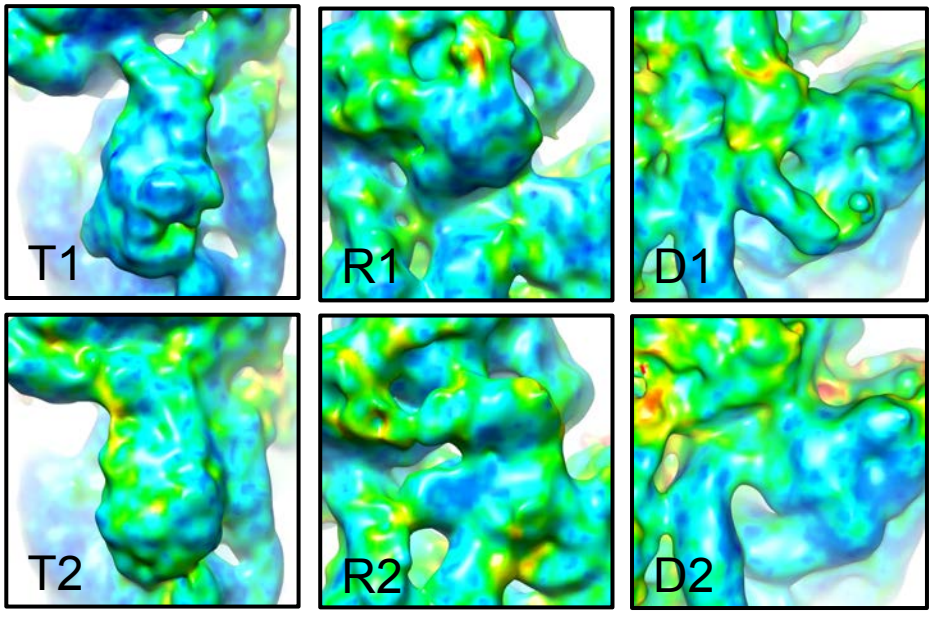

Legend: From the final Rio2-TAP refinement, focused 3D classification identified bimodal interface AF positions for Tsr1 (T1/T2) and Rio2 (R1/R2), along with Dim1 bound (D1) and unbound (D2) structures. Each AF local classification took place in two stages, first identifying the major two populations and then identifying the best particles of each.

Figure S3, related to Figure 4: Dim1 Electrostatics. A. Dim1, docked into pre-40S, shows one neutral face and another highly charged face. Electrostatics were calculated with in Chimera. **B.** Dim1 was positioned according to the position of its active site and point variants shown to affect binding. The position of R233-K236 is marked with a green ball. **C.** The Dim1-containing map with the Dim1 density removed via segmentation subtraction in Chimera. **D.** The same region but from the structure that is lacking Dim1, highlighting differences in the h45 region between Dim1-bound and Dim1-minus pre-40S ribosomes.

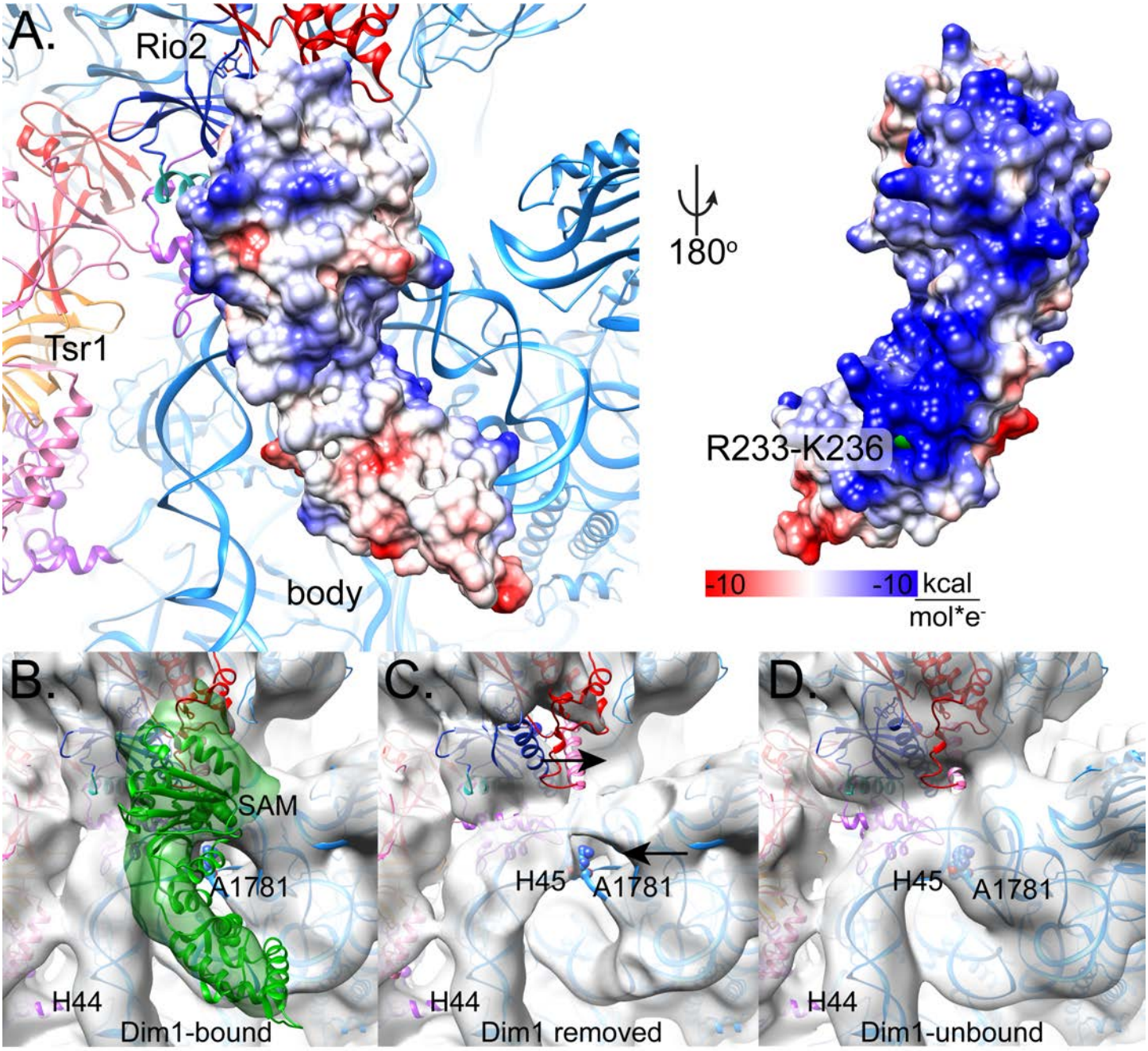

Figure S4, related to Figures 2 and 4: Model of 80S-like ribosomes. By superimposing Rps21, which is far from the interface, eIF5B-containing 80S ribosome fits over Rio2 and three of Tsr1's four domains. Dim1 conflicts with the rRNA. At least Rio2 and Tsr1 are found together with eIF5B in 80S-like ribosomes that represent an assembly intermediate that appears involved in proofreading. Rotation of Tsr1 away from the large subunit, towards the platform, akin to the movement from T1 (**A.**) to T2 (**B.**), would allow both Tsr1 and eIF5B to bind simultaneously.

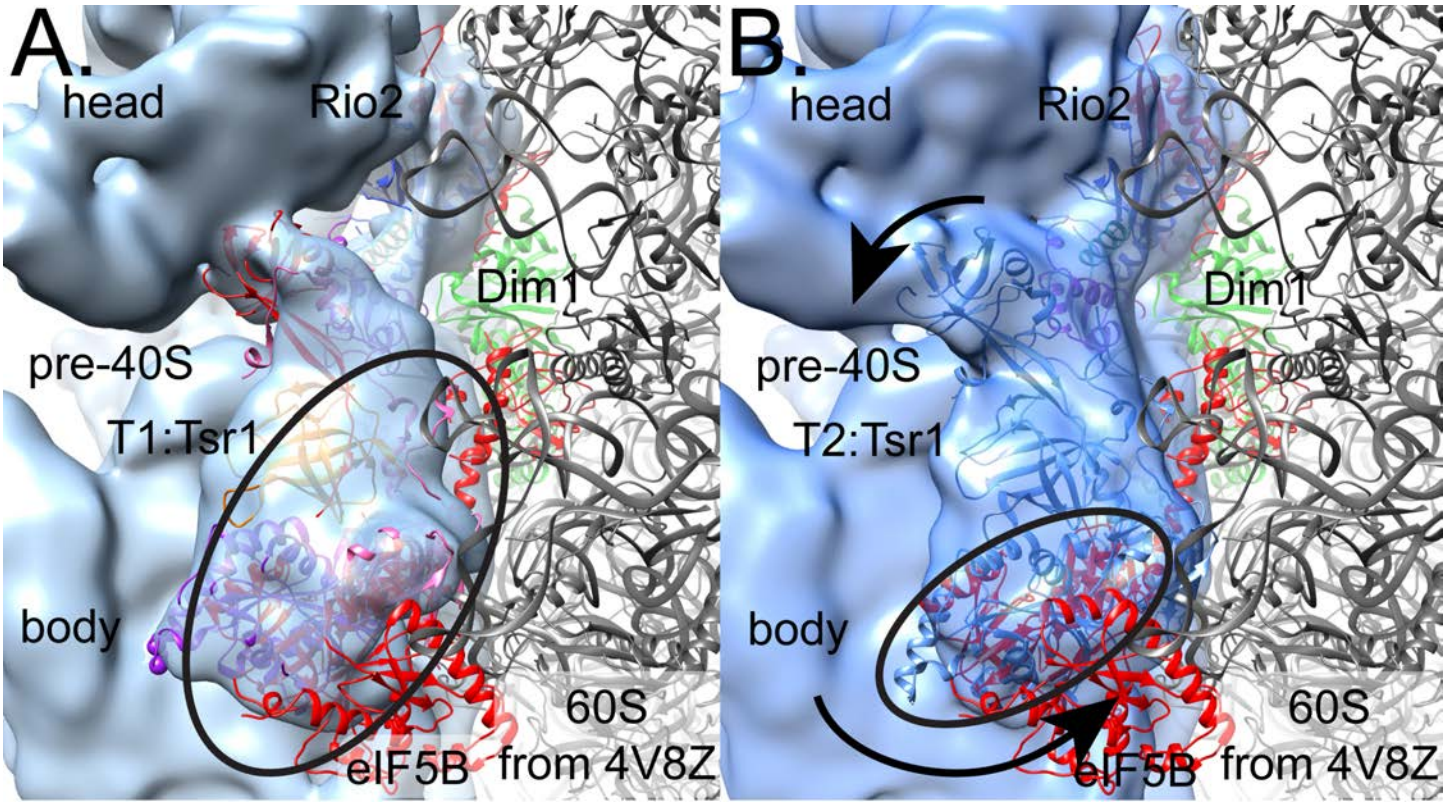

Figure S5, related to Figure 5: Focused classification of Ltv1-TAP platform AFs

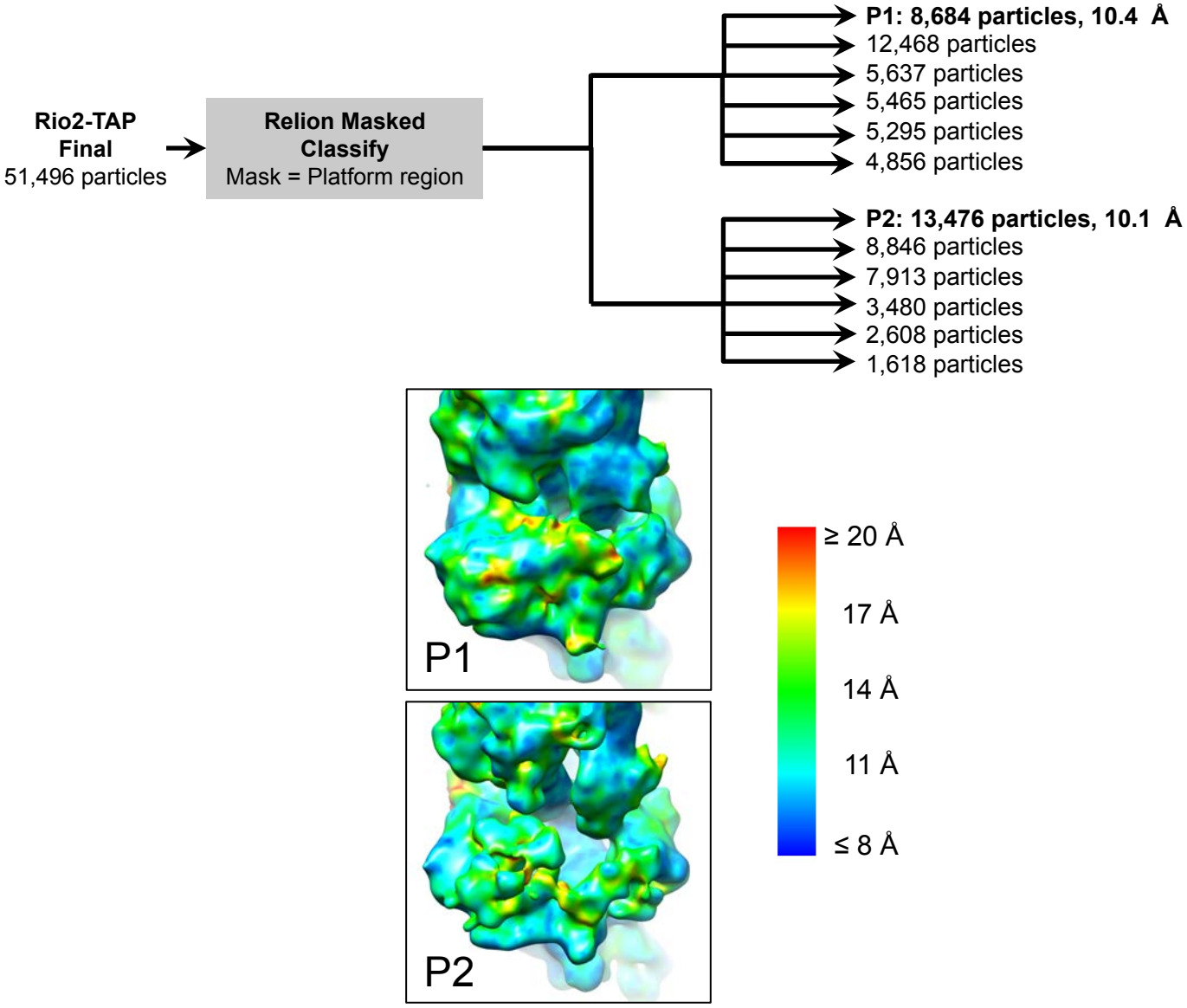

Legend: From the final Ltv1-TAP refinement, focused classification identified classes where the putative Nob1 density was either present or absent. A second generation of focused classification revealed several classes in which both Pno1 and Dim1 were present (P1), as well as several classes in which only Pno1, but not Nob1, was present (P2).

Figure S6, related to Figure 6: Coomassie-stained SDS-PAGEs of protein binding assays and Western blot analyses of AFs and their variants. The pulled down fractions shown are: I, input; F, flow-through; W, final wash; and E, eluted. **A.** The N-terminal fragment of Ltv1 ($Ltv1^N$) does not bind to Enp1 or MBP (control). **B.** $Ltv1^N$ binds to SUMO-Rps3 but not to the Ni-NTA resin. **C.** The Ltv1 core fragment ($Ltv1^M$) is sufficient for binding to SUMO-Rps3. **D.** Double-affinity purification of His_6-Rps3/Ltv1-Flag complex over Ni-NTA and Flag resins. The N-terminal KH domain of Rps3 interacts with Ltv1. The dotted line represents a lane of the gel that was irrelevant to the experiment and was, thus, digitally deleted. **For E-I:** Numbers on the right indicate the molecular weight markers. Pno1 is used as loading control in A and Tsr1 in B-E. Western blot analyses of total cell lysates from **E.** Tsr1 (WT) and its mutant (KKRR). **F.** Dim1 (WT) and its mutant (RKNK). **G.** Pno1 (WT) and its mutant (KKKF). **H.** Enp1 (WT) and its mutant (KKY). **I.** Ltv1 (WT) and its truncations N- Ltv11-180, M- Ltv1185-394.

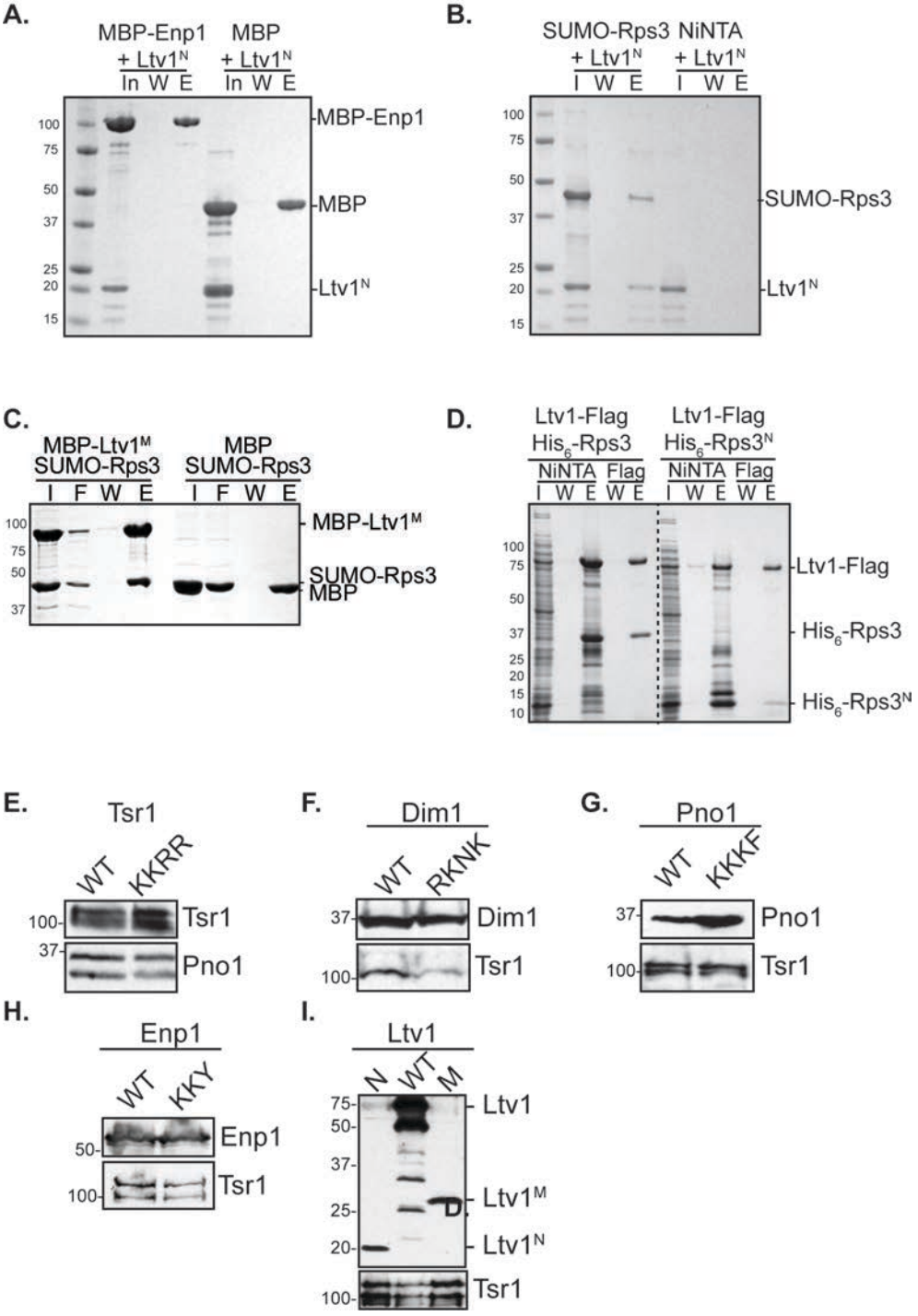

Table S1. Protein structure models used in this study, related to Figures 2-6

Each AF was modeled in our cryo-EM map using one of the following X-ray crystal or computational models.

AF	PDB	Model	Species
Tsr1	5IW7	n/a	*S. cerevisciae*
Rio2	4GYG	n/a	*C. thermophilum*
Dim1	1ZA9	n/a	*H. sapien*
Nob1	2LCQ	n/a	*P. horikoshii*
Pno1	3AEV	n/a	*P. horikoshii*
Rps3	4V88	n/a	*S. cerevisciae*
Enp1-TPR	n/a	Phyre	n/a

Table S2. Yeast strains used in this study, related to Figures 2, 4, 5, and 6

Some biochemical experiments were performed using recombinant yeast strains, summarized here.

Strain	Description	Genotype	Reference
YKK87	Rio2TAP	BY4741; Rio2TAP::His	Open Biosystems
YKK88	Ltv1TAP	BY4741; Ltv1TAP::His	Open Biosystems
YKK73	ΔLtv1	BY4741; Ltv1::KAN	Open Biosystems
YKK352	Rio2TAP; ΔLtv1	BY4741; Rio2TAP::His; Ltv1::KAN	(Strunk et al., 2011)
YKK427	GAL1::Enp1	BY4741; GAL1Enp1::KAN	This work
YKK487	GAL1::Pno1	BY4741; GAL1Pno1::KAN	This work
YKK410	GAL1::Dim1	BY4741; GAL1Dim1::KAN	This work
YKK367	Ltv1TAP; GAL1::Tsr1	BY4741; Ltv1TAP::His; GAL1Tsr1::KAN	(Strunk et al., 2011)

Table S3. Vectors used in this study, related to Figures 2, 4, 5 and 6

Some biochemical experiments were performed using the recombinant DNA vectors summarized here.

Vector	Description	Vector information	Reference
pKK193	pSV272-Ltv1	kan^r, T7 promoter, lac operator	(Campbell and Karbstein, 2011)
pKK1316	pSV272-$Ltv1^M$ (185-394)	kan^r, T7 promoter, lac operator	This work
pKK1313	pSV272-$Ltv1^N$ (1-180)	kan^r, T7 promoter, lac operator	This work
pKK199	pSV272-Enp1	kan^r, T7 promoter, lac operator	(Campbell and Karbstein, 2011)
pKK1317	pSV272-$Enp1^{TPR}$ (154-483)	kan^r, T7 promoter, lac operator	This work
pKK1432	pETDuet-1- His6-Rps3/ Ltv1-Flag	amp^r, T7 promoter, lac operator	This work
pKK1434	pETDuet-1-His6-$Rps3^N$(1-95)/ Ltv1-Flag	amp^r, T7 promoter, lac operator	This work
pKK1230	pET28-SUMO-Rps3	kan^r, T7 promoter, lac operator	(Ghalei et al., 2015)
pKK3541	pRS416- Enp1	amp^r, CEN, Ura3, TEF promoter, CYC1 terminator	This work
pKK3797	pRS416- Enp1_K378E,K379E,Y380I	amp^r, CEN, Ura3, TEF promoter, CYC1 terminator	This work
pKK3270	pRS416- Pno1	amp^r, CEN, Ura3, TEF promoter, CYC1 terminator	This work
pKK3275	pRS416- Pno1-ΔN (87-274)	amp^r, CEN, Ura3, TEF promoter, CYC1 terminator	This work
pKK3823	pRS416- Pno1_K208E,K211E,K213E, F214A	amp^r, CEN, Ura3, TEF promoter, CYC1 terminator	This work
pKK3295	pRS416- Tsr1	amp^r, CEN, Ura3, TEF promoter, CYC1 terminator	This work
pKK3764	pRS416- Tsr1_K201E,K203E,R245E,R248E	amp^r, CEN, Ura3, TEF promoter, CYC1 terminator	This work
pKK3146	pRS416- Dim1	amp^r, CEN, Ura3, TEF promoter, CYC1 terminator	This work
pKK3836	pRS416- Dim1_R233E,K234E,N235D,K236E	amp^r, CEN, Ura3, TEF promoter, CYC1 terminator	This work

Movie 1, related to Figure 2: Conformational changes in Tsr1. Tsr1 exists in at least two discrete positions, one that does not contact h44 (T1) and another that does (T2). The two conformations are related to one another by a ~28^{o} rotation. We used the “morph” command in Chimera to move between the positions to help visualize the change.

Movie 2, related to Figure 3: Conformational changes in Rio2. Rio2 exists in at least two discrete positions, one that is elongated (R1) and another that is U-shaped (R2). The two conformations are related to one another by opening at the ATP biding cleft. We used the “morph” command in Chimera to move between the positions to help visualize the change.